International Journal of Microwave and Wireless Technologies

cambridge.org/mrf

Toward practical activation of nonreciprocal metasurfaces: dual control and design framework

Kazuhiro Takahagi and Alan Tennant

School of Electrical & Electronic Engineering, University of Sheffield, Sheffield, UK

Research Paper

Cite this article: Takahagi K, Tennant A (2026) Toward practical activation of nonreciprocal metasurfaces: dual control and design framework. *International Journal of Microwave and Wireless Technologies* **18**(3), 375–383. https://doi.org/10.1017/S1759078726102888

Received: 19 September 2025
Revised: 14 January 2026
Accepted: 16 January 2026
First published online: 4 February 2026

Keywords:
electromagnetic absorption; electromagnetic metamaterials; metasurfaces

Corresponding author: Kazuhiro Takahagi; Email: ktakahagi1@sheffield.ac.uk

Abstract

This paper presents an actively controllable nonreciprocal metasurface based on a ferrite–patch structure with PIN diodes for dynamic control. Two activation methods are investigated: (a) phase control, which enables a 30° transmission-phase shift while maintaining nonreciprocal behavior, and (b) ON–OFF control, which switches the response by altering the propagation path. The phase-control metasurface is analyzed using transmission-line theory, full-wave simulation, and experiments, showing good agreement across methods. The ON–OFF design is optimized to suppress bidirectional transmission when ON. Experimental results confirm strong nonreciprocity, though slight frequency shifts arise from FR4 variability, and a back-fitted simulation improves consistency. The proposed dual-control framework provides a compact and low-cost approach to reconfigurable nonreciprocal surfaces that retain the use of permanent magnets for ferrite bias and are applicable to microwave wireless systems, including adaptive isolation, interference control, and tunable shielding. The results demonstrate the feasibility of compact, reconfigurable nonreciprocal metasurfaces using simple biasing circuits and offer design insights for frequency-stable implementations.

Introduction

Research on metasurfaces as a means of controlling electromagnetic waves has been extensively conducted, particularly for applications in antennas [1] and electromagnetic absorbers [2]. These structures have evolved as a technology for thinning and miniaturizing wavelength-dependent electromagnetic control materials, which is essential for electromagnetic interference suppression and antenna performance enhancement. Furthermore, metasurfaces offer effective approaches for realizing electrically compact antennas and achieving high gain. In recent years, methods for actively controlling electromagnetic waves by combining metasurfaces with active circuit elements – referred to as reconfigurable intelligent surfaces (RIS) – have attracted significant attention [3, 4]. RIS technology provides a cost-effective and lightweight alternative for electronic beam steering of antennas and is regarded as a promising direction in electromagnetic wave manipulation. Fundamentally, RIS is composed of a periodic arrangement of metallic patches (metasurfaces) integrated with electronically controllable active components, allowing control of reflection and transmission phase at the unit-cell level. As a result, there is a growing demand for metasurfaces that enable dynamic control of electromagnetic behavior via electrical signals. The fundamental mechanisms for wave manipulation include reflection, transmission, and absorption. In general, these mechanisms are reciprocal, meaning that electromagnetic characteristics remain unchanged with respect to the direction of propagation across the same planar structure [5]. However, there is a growing demand for nonreciprocal behavior, in which different responses are exhibited depending on the direction of incidence at the same frequency. Such functionality is highly desirable for interference mitigation and spatial filtering. Recent studies have proposed nonreciprocal surfaces using amplifier–antenna combinations [6] or through the use of magnetically biased materials [7], indicating a promising research direction. Our group has been investigating a simple structure that achieves nonreciprocity by combining ferrite materials with metallic patches [8], and we have demonstrated a structure that exhibits high transmission with substantial isolation. However, characteristics such as frequency response and isolation level are inherently fixed by the physical properties of the ferrite and the electromagnetic characteristics of the metallic patch, thus limiting external control capabilities. While electromagnetic coils can be used to modulate the magnetic bias field applied to ferrites [9], practical implementation is hindered by power consumption and thermal management issues. To address this, we propose an electrically controllable method for nonreciprocal behavior by loading PIN diodes onto the metallic

© The Author(s), 2026. Published by Cambridge University Press in association with The European Microwave Association.

patch array. This paper introduces a dual control approach for activating nonreciprocity using PIN diodes – one method for phase control and another for direct modulation of nonreciprocity. We present the design methodology and experimental validation of these approaches based on fundamental operating principles. The proposed nonreciprocal metasurface retains a static magnetic bias for ferrite activation, while adding electrical tunability through PIN-diode control, enabling compatibility with microwave wireless systems such as adaptive isolation surfaces, reconfigurable interference-suppression layers, and tunable electromagnetic shielding. These application scenarios motivate the development of the controllable nonreciprocal mechanisms presented in this work. A preliminary version of this work was presented at EuCAP 2025, focusing on active phase control through simulation and experiment [10]. In this extended version, we add transmission-line analysis to clarify the operating principle and enhance the design. Moreover, we introduce a new ON–OFF control scheme, further advancing the versatility of nonreciprocal metasurface design.

Principle of nonreciprocal metasurfaces

Electromagnetic characteristics of ferrite

The key element of the proposed nonreciprocal metasurface is a thin cylindrical ferrite material, referred to here as a ferrite disk. Ferrite disks are commonly used in waveguide-type circulators and isolators and are known to exhibit rotational propagation characteristics when a static magnetic field is applied. As illustrated in Fig. 1(a) and (b), when a magnetic bias is applied parallel to the height (z-axis) of a ferrite cylinder, the material exhibits clockwise or counterclockwise rotational propagation behavior depending on the magnetic field direction, for incoming electromagnetic waves polarized in the same direction (in this case, vertically polarized waves). Typically, the magnetic field is provided by permanent magnets placed above and below the ferrite disk, allowing the direction of the bias field to be controlled by flipping the magnets. When the magnetic field is fixed to produce clockwise propagation within the center of the metasurface unit cell, an incident wave arriving from the direction of the blue arrow in Fig. 1(a) propagates through the blue-shaded region on the left. Conversely, a wave incident from the direction of the red arrow propagates through the red-shaded region on the right. Reversing the magnetic field results in the mirrored configuration shown in Fig. 1(b). A simplified model of a passive nonreciprocal unit cell is shown in Fig. 1(c). It consists of metallic lines or patches on a dielectric substrate. In this configuration, the blue region in Fig. 1(a) corresponds to the metal line, while the red region represents a void or gap within the substrate. The ferrite's rotational propagation occurs only within a frequency band determined by its material parameters and diameter; outside this range, wave behavior is dominated by the patterned metal and gaps. Therefore, for practical metasurface design using patterned metal, it is desirable to implement only one of the two structures per unit cell. When a cylindrical ferrite is employed in circulators or isolators, nonreciprocity is typically achieved by utilizing anisotropic permeability to equalize the phase velocities of right-handed and left-handed circularly polarized waves. This makes it possible to select the desired output port based on the rotation angle of the wave [11]. The optimum ferrite radius R for rotational propagation at a given frequency is given by equation (1) [12]:

$$R = \frac{1.84\lambda}{2\pi\sqrt{\mu\varepsilon}}, \tag{1}$$

where μ is the effective permeability, Ɛ is the permittivity, and λ is a wavelength of operating frequency band. To realize rotational propagation for plane waves, the array response must be optimized through full-wave electromagnetic simulation based on this ferrite radius. In this study, CST Studio Suite (F-solver) is used for the electromagnetic simulation. The structure analyzed consists of an infinite array of ferrite disks placed on a plane, as shown in Fig. 1(d). At frequencies supporting rotational propagation, the incident wave penetrates the ferrite and experiences slight absorption, whereas outside this band the ferrite disks have little effect, particularly for sparse arrays. Therefore, simulations neglecting inter-element spacing yield qualitatively similar results. In this study, we focus on the 6 GHz band as the operating frequency, and we adopt ferrite materials with the following specifications based on prior experimental validation [8]: diameter 7.5 mm, relative permittivity of 15, relative permeability of 1.1, saturation magnetization of 1600 Gauss, and an applied bias field of 650 Gauss. The simulation result in Fig. 2 confirms slight absorption around 6.5 GHz, near the center of the targeted band. Because this ferrite-only array does not include patterned metal, it exhibits rotational propagation but remains reciprocal. Henceforth, we assume the bias magnetic field is oriented upward, resulting in clockwise propagation for all models discussed.

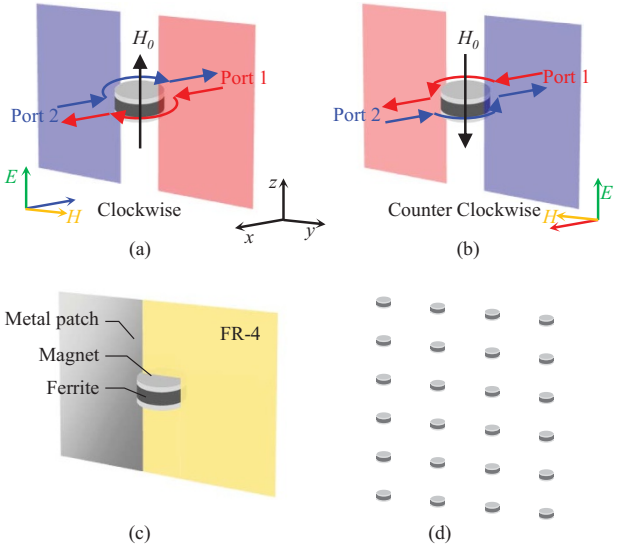


Figure 1. Unit cell structure of the proposed nonreciprocal metasurface and operation principle of the ferrite disk.

Design of active control

For the activation of nonreciprocal metasurfaces, two approaches are considered: (a) controlling the phase response of nonreciprocal transmission, and (b) switching the presence or absence of nonreciprocal behavior using an ON–OFF control scheme. The first approach, phase control, aims to realize a nonreciprocal transmission similar to the passive case, where one direction is always blocked and the other always transmits, as shown in Fig. 3(a). In this configuration, the blocked direction (Port 1) corresponds to propagation through the gap side, which is opposite to the metallic patch. This ensures that the signal is suppressed regardless of the ON or OFF state of the PIN diode. On the other hand, for

https://doi.org/10.1017/S1759078726102888 Published online by Cambridge University Press

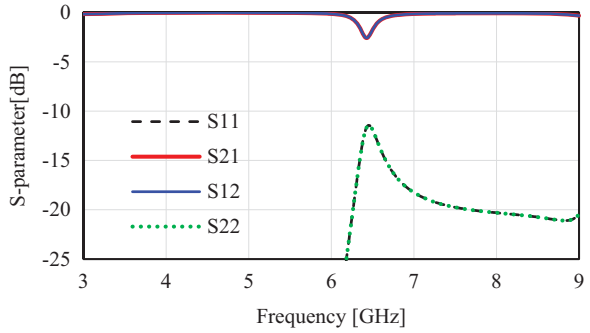


Figure 2. Simulated S-parameters of a ferrite disk array using full-wave analysis.

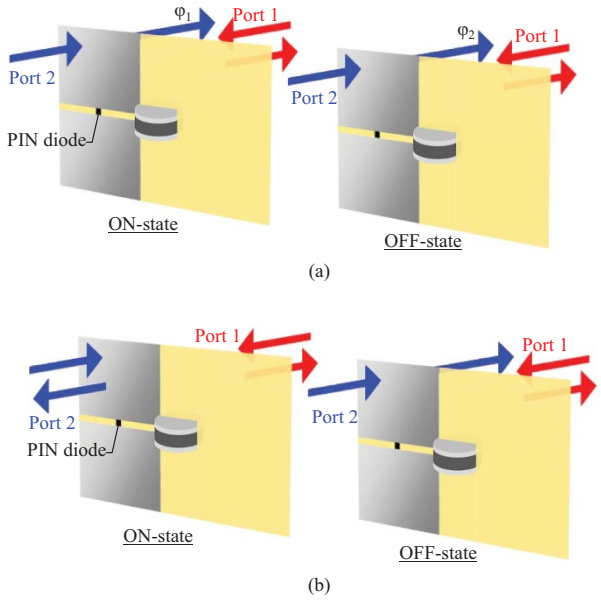


Figure 3. Types of active nonreciprocity control: (a) phase control method, (b) ON–OFF switching of nonreciprocal behavior.

the transmitting direction (Port 2), the wave propagates through the metallic patch side. In this case, a PIN diode is embedded on the patch, and the goal is to achieve phase variation depending on the diode's switching state. This enables dynamic phase control while maintaining the inherent nonreciprocity. The second approach directly switches the nonreciprocity itself. As illustrated in Fig. 3(b), Port 1 remains suppressed as in the first method, whereas Port 2 is designed to transmit when the diode is OFF and to form a stopband when the diode is ON, allowing the overall behavior to toggle between nonreciprocal and reciprocal states.

In this paper, we verify the feasibility of both control strategies through electromagnetic simulations using CST Studio Suite and analytical design based on transmission-line theory. Experimental validation using minimum-sized metasurface arrays is also conducted, and the results are discussed in the following sections.

Phase control of nonreciprocity

Unit cell structure

As the first control approach, we investigate a method for modulating the transmission phase of an already established nonreciprocal response. The proposed active unit cell structure for phase control

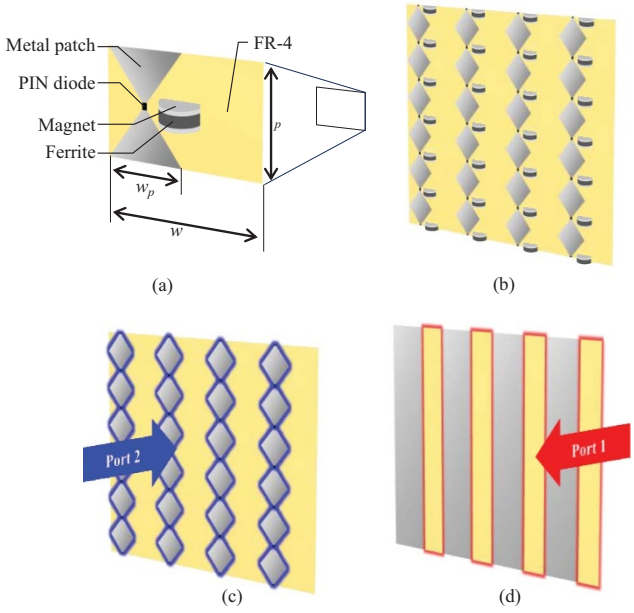


Figure 4. Phase control of nonreciprocal metasurface: (a) unit cell structure, (b) overall array layout, (c) assumed propagation structure for Port 2, (d) assumed propagation structure for Port 1.

is illustrated in Fig. 4(a). The unit cell has a width $w = 26$ mm, a patch width of 12.9 mm, and a height $p = 16.25$ mm, which includes the rhombic patch height of 15.25 mm and a gap of 1 mm. The metallic patch is configured in a rhombus shape, with a PIN diode connected at the vertex. This geometry is selected for ease of impedance matching. The PIN diode used in this study is the BAP50-03, for which several literature reports [13, 14] model its ON and OFF states as follows:

- ON state: A series R–L circuit with resistance $R = 2.1\,\Omega$ and inductance $L = 0.6$ nH.
- OFF state: A series L–C circuit with the same $L = 0.6$ nH and capacitance $C = 0.17$ pF.

The ferrite element is placed at the center of each unit cell, and the overall metasurface array is shown in Fig. 4(b). For input from Port 2 (metallic-patch side), the wave propagates through the rhombic patch array and interacts with both the patch and PIN diode, making their electromagnetic properties dominant, as depicted in Fig. 4(c). In contrast, input from Port 1 primarily travels through the air-gap side, which effectively behaves as a continuous metallic strip surrounding the gap, as shown in Fig. 4(d). Consequently, the wave propagation in this direction can be interpreted as occurring along a simplified transmission line formed by the void region.

Transmission-line theory analysis

The equivalent circuits corresponding to each propagation configuration are shown in Fig. 5. Figure 5(a) and (b) represent the equivalent circuits when the PIN diode is in the OFF and ON states, respectively. The regions enclosed by dashed lines represent the equivalent models of the diode. In these circuits, the reactance X_L represents the inductive component of propagation through the patch, while the susceptance B_C corresponds to the capacitive coupling between adjacent patches. For a rhombic patch array, these

https://doi.org/10.1017/S1759078726102888 Published online by Cambridge University Press

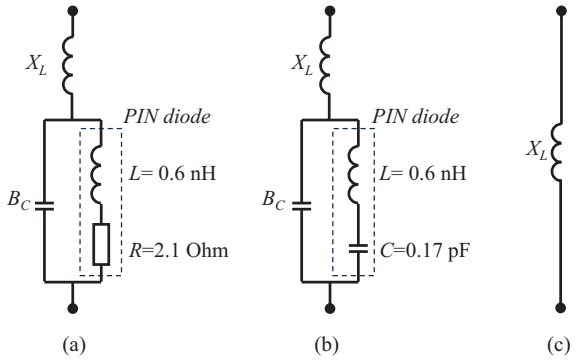


Figure 5. Equivalent circuit models: (a) Port 2 with diode ON, (b) Port 2 with diode OFF, (c) Port 1 equivalent circuit.

parameters are derived by considering a 45-degree rotated square patch array, resulting in values approximately scaled by $1/\sqrt{2}$. The inductive and capacitive components of the square patch array can be calculated using equations (2) and (3) [15, 16]:

$$\frac{X_L}{Z_0} = F\left(\mathrm{w}, w_p, \lambda, \theta\right) = \frac{\mathrm{w}\ cos\theta}{\lambda}\left\{1n\ csc\frac{\pi w_p}{2w} + G\left(w,w_p,\lambda,\theta\right)\right\} \tag{2}$$

$$\frac{B_C}{Z_0} = 4F\left(\mathrm{p}-\mathrm{g}, \mathrm{p}, \lambda, \theta\right) = \frac{(\mathrm{p}-\mathrm{g})\ cos\theta}{\lambda} \left\{1n\ csc\frac{\pi p}{2\left(p-g\right)} + G\left(p-g,p,\lambda,\theta\right)\right\} \tag{3}$$

where, w is the unit cell width, w_p is the patch width, p is the cell height, and g is the gap between patches. The parameter $G(w, w_p, \lambda, \theta)$ used in equations (2) and (3) is computed from equations (4) through (6):

$$G\left(w, w_p, \lambda, \theta\right) = \frac{1}{2}\frac{\left(1-\beta^2\right)^2\left[\left(1-\frac{\beta^2}{4}\right)\left(A_+ + A_-\right) + 4\beta^2 A_+ A_-\right]}{\left(1-\frac{\beta^2}{4}\right) + \beta^2\left(1+\frac{\beta^2}{2}-\frac{\beta^4}{8}\right)\left(A_+ + A_-\right) + 2\beta^6 A_+ A_-}, \tag{4}$$

$$A_\pm = \frac{1}{\sqrt{1 \pm \frac{2\mathrm{w}\ sin\theta}{\lambda} - \left(\frac{\mathrm{w}\ cos\theta}{\lambda}\right)^2}} - 1 \tag{5}$$

$$\beta = sin\frac{\pi w_p}{2w}. \tag{6}$$

Using the calculated reactance and susceptance, the impedance Z is determined by

$$Z = jX_L + \frac{1}{jB_C}. \tag{7}$$

Then, based on the admittance Y, the reflection coefficient S_{11} and transmission coefficient S_{21} are calculated using equations (8) through (11):

$$Y = Z^{-1}, \tag{8}$$

$$|T|^2 = \frac{4}{4+|Y|^2}, \tag{9}$$

$$S_{11} = 10log\left(1-|T|^2\right), \tag{10}$$

$$S_{21} = 10log\left(|T|^2\right). \tag{11}$$

Note that transmission-line theory assumes reciprocity, and therefore the expressions for S_{11} and S_{21} are shown here for convenience. However, in the context of our design, the forward and reverse directions correspond to structurally distinct propagation paths as shown in Fig. 4(c) and (d). Thus, the values obtained are treated as S_{12} and S_{22}, respectively, depending on the direction of analysis. For propagation from Port 1, the wave primarily passes through the air-gap side, which can be modeled as a purely reactive structure. Therefore, the corresponding equivalent circuit is shown in Fig. 5(c), and the impedance can be approximated using equation (2) alone. The results of the transmission-line analysis are shown in Fig. 6. Figure 6(a) presents the result for the diode ON state, while Fig. 6(b) shows the diode OFF state. The transmission phase difference between these states is plotted in Fig. 6(c). As described in Section 2, the ferrite's rotational propagation characteristic operates primarily around 6.5 GHz within the 6 GHz band. Thus, for Port 1 – the blocked direction – the 6.5 GHz value is used as the representative response. As shown in Fig. 6(a), the ON-state circuit exhibits a high-pass filter characteristic similar to a metal strip line array. The simulation predicts a clear suppression of transmission from Port 1 at 6.5 GHz, representing the desired nonreciprocal behavior.

In contrast, as shown in Fig. 6(b), the OFF-state circuit exhibits a cutoff near 5 GHz, transitioning to transmission in the 6 GHz band. This configuration results in nonreciprocal isolation, with suppression occurring only for Port 1. Figure 6(c) indicates an S_{12} phase shift of approximately 40 degrees between ON and OFF states. Although the model does not include ferrite, the result confirms the feasibility of phase control.

Simulation results

Electromagnetic simulations were conducted using the unit-cell analysis feature of the F-solver in CST Studio Suite, assuming an infinite periodic structure. The ferrite parameters used in the model are consistent with those described in Section 2, while the characteristics of the PIN diode were modeled using CST's Schematic simulation environment. Figure 7(a) shows the result when the diode is in the ON state. A strong nonreciprocal behavior is observed near 6.5 GHz, with a transmission level of – 0.6 dB and a rejection level exceeding – 11 dB. This behavior closely resembles that of previously reported passive-type nonreciprocal metasurfaces without PIN diodes [8]. The reason for this is that, under the ON condition, the metallic structure behaves as a continuous conducting surface, producing behavior consistent with the high-pass filter characteristics predicted by the transmission-line theory in Fig. 6(a). In contrast, Fig. 7(b) shows the result when the diode is in the OFF state. At the same frequency (~6.5 GHz), a transmission level of—2.3 dB and a rejection level better than – 17 dB were achieved, indicating strong nonreciprocal behavior. The slight reduction in transmission level compared to the ON case is attributed to the impedance shift caused by the diode's OFF-state characteristics, which move the passband of the metallic patch structure toward higher frequencies. The stopband appears around 5 GHz, in good agreement with the result predicted by transmission-line analysis. However, when compared to Fig. 6(b), the simulation result reveals a reversal in transmission and reflection characteristics in the 6 GHz nonreciprocal band. This discrepancy arises because the CST simulation more accurately models

https://doi.org/10.1017/S1759078726102888 Published online by Cambridge University Press

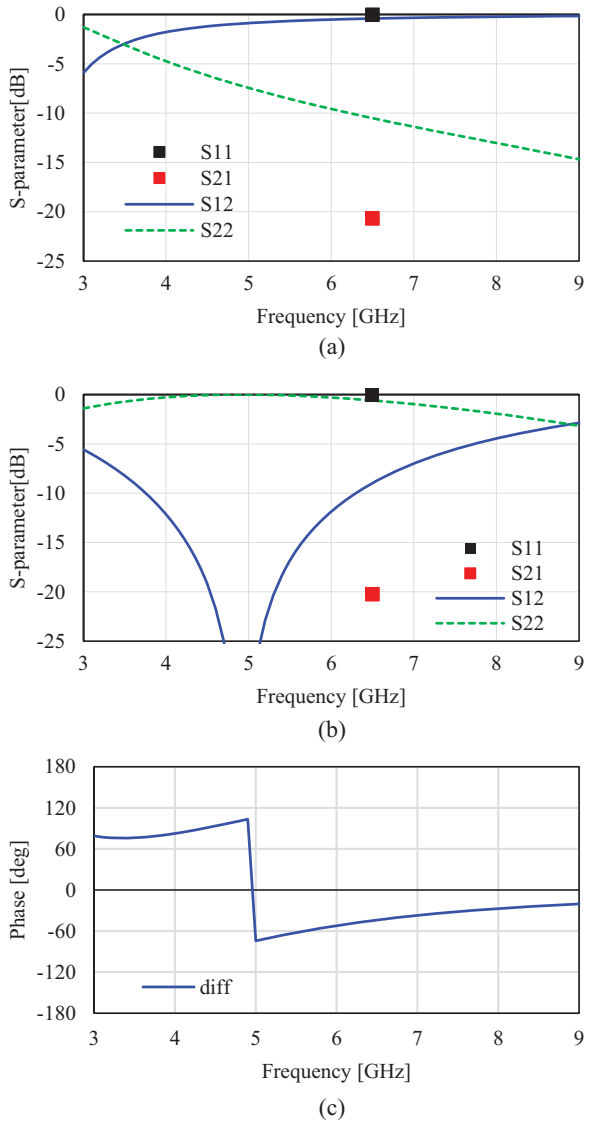


Figure 6. Transmission-line analysis results: (a) diode ON, (b) diode OFF, (c) phase difference of S_{12}.

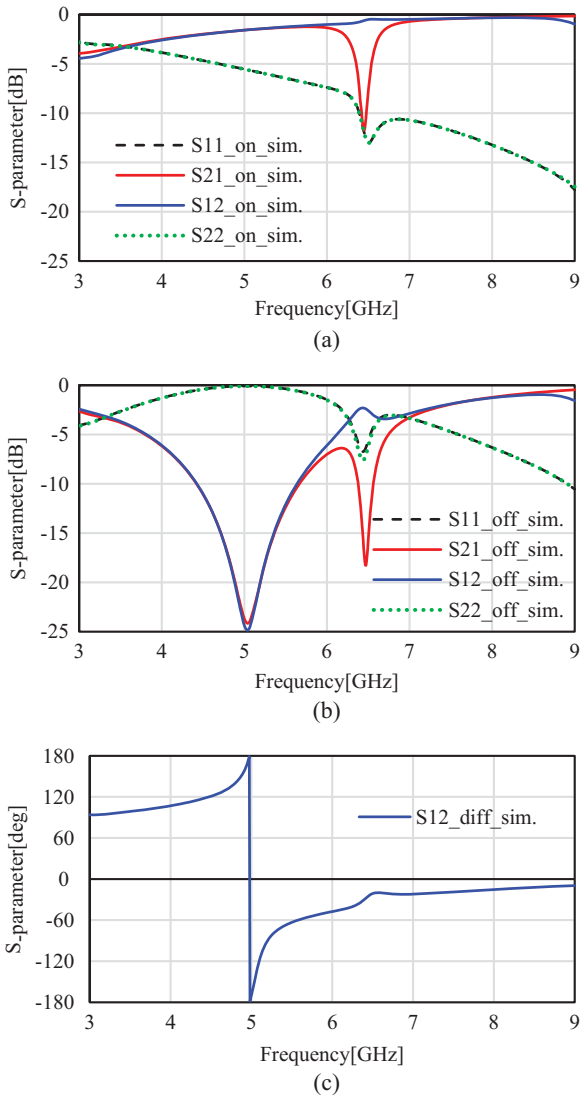


Figure 7. Full-wave simulation results: (a) transmission and isolation with diode ON, (b) transmission and isolation with diode OFF, (c) transmission phase difference (S_{12}) between ON and OFF states.

the full 3D geometry, whereas the analytical model assumes a simplified strip line approximation. The phase difference in the transmission, shown in Fig. 7(c), also resembles the behavior in Fig. 6(c), exhibiting an approximate phase shift of 30 degrees. This is likely due to enhanced transmission through the ferrite, which affects the phase response. While a binary phase shift of 180 degrees is desirable for ideal phase control, the observed result demonstrates meaningful differentiation at this preliminary stage of design. Importantly, the simulation results confirm that even with the inclusion of PIN diodes in the metallic patches, the nonreciprocal operating frequency remains unchanged, and transmission continues to occur in the same direction, validating the effectiveness of the proposed design.

Experimental results

An experimental model of the phase-controllable nonreciprocal metasurface was fabricated using a 1.6 mm-thick FR4 substrate with copper foil patches and ferrite elements manufactured by Molex. The metasurface consisted of a 3 × 3 array, as shown in Fig. 8. DC bias for the PIN diodes was applied across the upper and lower sides of the patches, and in the ON state a voltage of 5 V and current of 10 mA were supplied to all three rows simultaneously. The fabricated sample was placed between a pair of horn antennas, and S-parameters were measured using a vector network analyzer (Agilent 8532B). To stabilize the field distribution while avoiding physical interference with the small 3 × 3 sample, a metal shielding plate with a center aperture was used. Figure 9(a) shows the ON-state result. A sharp nonreciprocal response appears near 6.6 GHz, with a transmission level of – 1.8 dB and isolation of – 14 dB, closely matching the simulation in Fig. 7(a). In the OFF state, shown in Fig. 9(b), a transmission level of – 7.2 dB and isolation of – 24 dB were observed, indicating a similar trend to Fig. 7(b) despite the reduced transmission magnitude. Two factors account for this reduction. First, the OFF-state bandpass frequency shifted upward, placing 6.5 GHz near the transition between the stopband and passband. Second, periodic ripple-like dips occurred in both states due to multi-path interference between

https://doi.org/10.1017/S1759078726102888 Published online by Cambridge University Press

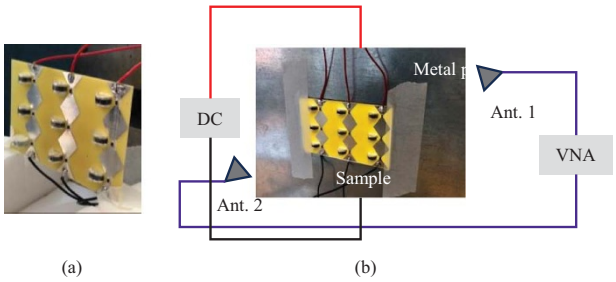


Figure 8. Fabricated prototype of the nonreciprocal metasurface used for transmission phase control experiment, (a) model (b) set-up.

the sample and the shielding plate. In both Fig. 9(a) and (b), results with and without ferrite loading are shown for comparison. Outside the ferrite's operational band (around 6.5 GHz, Fig. 2), the ON-state transmission and OFF-state stopband near 5 GHz remain essentially unchanged, confirming that nonreciprocity can be added to an existing metasurface simply by loading ferrite without modifying the original structure. Additionally, reverse-direction nonreciprocal behavior was observed near 7.8 GHz. This can be attributed to the ferrite's rotational propagation characteristics, which depend on the relationship between saturation magnetization and applied magnetic field. While the simulation assumes an ideal, uniform magnetic field, the experimental setup applies bias using finite-sized permanent magnets, which may introduce field nonuniformity or angular deviation, leading to reversed nonreciprocal behavior near the operating band. Regarding the phase shift, Fig. 9(c) shows a value of approximately 30°, consistent with the simulation in Fig. 7(c). Despite minor deviations, the overall experimental results validate the proposed concept and provide important insights for further improvement. The designed forward transmission level is approximately −3 dB (Fig. 6b), whereas Fig. 9(b) shows a lower measured value (around −8 dB) due to ripple and mismatch effects from the measurement fixture. Nevertheless, the overall nonreciprocal trend agrees with the simulation, and improved fixture conditions would yield transmission closer to the design value.

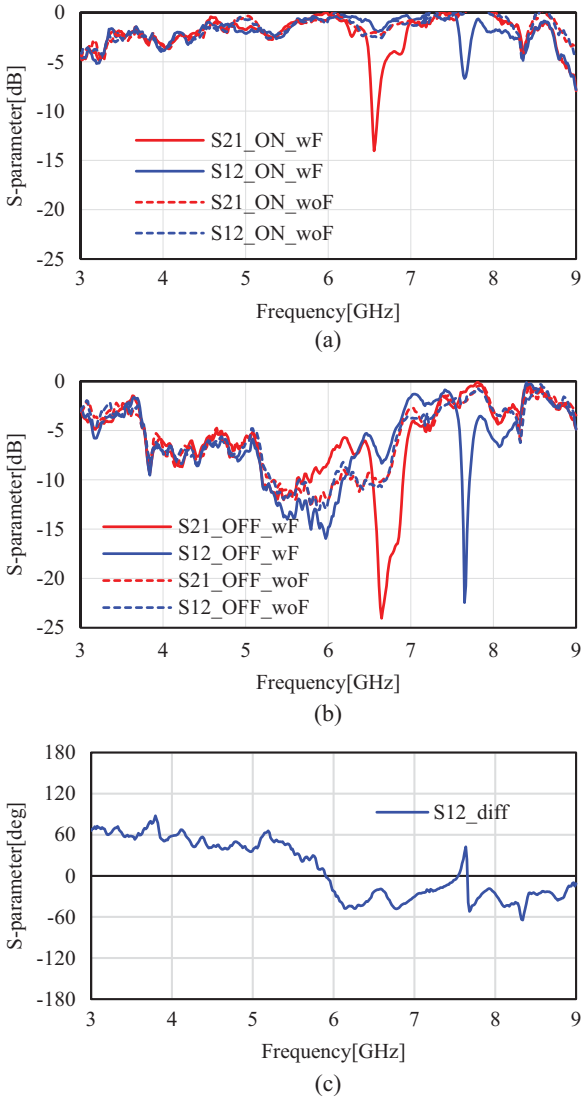


Figure 9. Experimental results: (a) with and without ferrite in diode ON state, (b) with and without ferrite in diode OFF state, (c) measured transmission phase difference between ON and OFF states.

On–OFF control of nonreciprocity

Simulation-based design

The second method for achieving active control of nonreciprocity – ON–OFF switching – is based on the configuration illustrated in Fig. 3(b), where the objective is to block the transmission path in the ON state. Specifically, the metasurface must behave as a band-pass structure in the OFF state, and transition to a band-stop structure in the ON state, thus disabling nonreciprocal transmission when the PIN diode is switched on. To realize this behavior, we optimized the unit cell geometry shown in Fig. 10(a). Through parameter sweeps using CST Studio Suite, the optimal dimensions were found to be: cell width $w = 45$ mm, patch width $w_p = 19$ mm, and cell height $p = 25$ mm. The required 45-mm cell width, which produces the stopband near 6.5 GHz in the ON state, is comparable to the wavelength at that frequency. Consequently, this dimension approaches the limit of equivalent-circuit models such as (2) and (3), which assume electrically small structures. For this design, we therefore rely solely on full-wave simulation. The results are shown in Fig. 11. Figure 11(a) presents the ON-state response, where a sharp stopband appears around 6.5 GHz, indicating that both Port 1 and Port 2 are strongly suppressed, i.e., the nonreciprocal response is canceled. In contrast, the OFF-state result in Fig. 11(b) shows clear nonreciprocity, with Port 2 maintaining transmission while Port 1 remains suppressed as intended. The reduced isolation observed in Fig. 11(b) can be explained by the physical mechanism that produces nonreciprocity in this structure. Forward transmission is governed by the geometric patch width, whereas backward propagation is influenced by ferrite-induced rotation, which effectively increases the apparent patch width by the ferrite diameter. At the operating frequency, the patch width is already near the limit of validity for the transmission-line model, and the ferrite-augmented width results in weaker mismatch in the backward direction, thereby lowering the isolation. Although this design sacrifices some isolation, it was intentionally adopted to ensure bidirectional suppression in the ON state and nonreciprocal behavior in the OFF state. Further optimization may improve the isolation, but the present performance sufficiently verifies the ON–OFF control concept.

https://doi.org/10.1017/S1759078726102888 Published online by Cambridge University Press

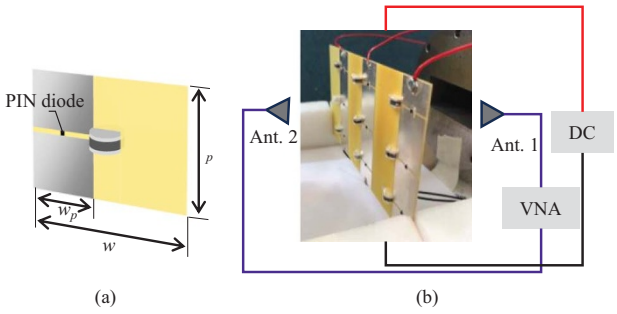


Figure 10. ON–OFF control metasurface model: (a) unit cell configuration, (b) fabricated prototype and measurement setup.

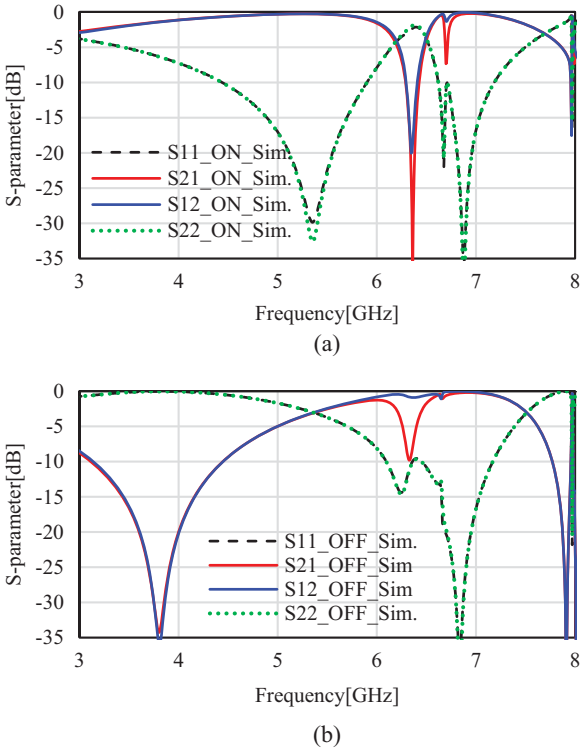


Figure 11. Simulation results: (a) ON-state response, (b) OFF-state response.

Experimental results and back-fitted simulation

The fabricated prototype for the ON–OFF controlled metasurface is shown in Fig. 10(b). The experimental setup follows the same configuration used for the phase-control measurements: a 3 × 3 array mounted within a metallic shielding plate to suppress edge diffraction and ensure stable measurement. The measured S-parameters are plotted as solid lines in Fig. 12. Figure 12(a) and (b) show the ON- and OFF-state results, respectively. In both states, nonreciprocal behavior appears near 6.5 GHz, although the ON-state stopband frequency shifts from the simulated value. This deviation likely arises from the square patch geometry, whose broader current distribution increases parasitic capacitance compared to the rhombic patch used in the phase-control design. To examine this effect, we performed back-fitted electromagnetic simulations by adjusting the substrate permittivity. The dashed curves in Fig. 12 represent these results. A permittivity increase of 1.3

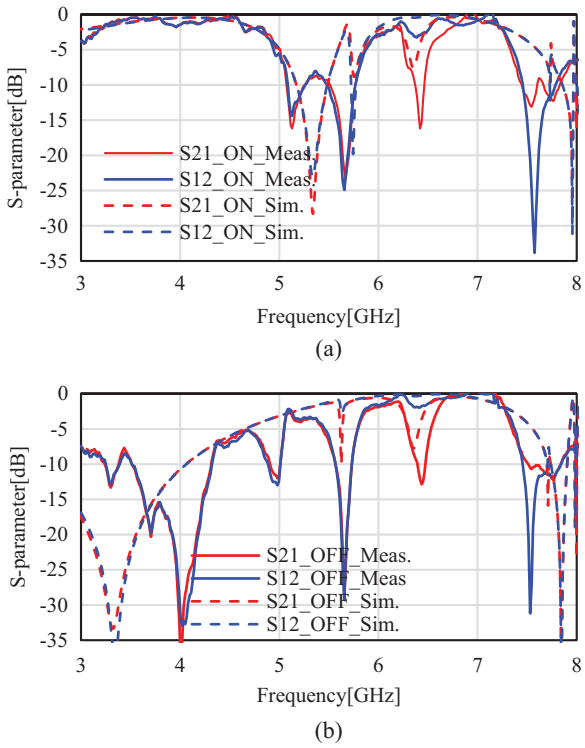


Figure 12. Comparison of experimental results (solid lines) and back-fitted simulations (dashed lines): (a) ON state, (b) OFF state.

yielded the best agreement, with the resonant dips and nonreciprocal features aligning closely with the measurements, particularly for the ON state in Fig. 12(a). Parasitic capacitance around the PIN-diode mounting may contribute to the deviation; however, variability in the dielectric constant of FR4 is considered the dominant factor, as such variations are widely reported [17], and the square-patch configuration is especially sensitive to them. These findings indicate that achieving sharp and repeatable stopband characteristics requires substrate materials with well-controlled permittivity.

The ON state was originally designed to exhibit a bidirectional stopband, suppressing both S_{21} and S_{12} at the operating frequency (Fig. 11a). However, in Fig. 12(a), a strong nonreciprocal response reappears near 6.5 GHz. This occurs because FR4 permittivity variations shift the stopband downward toward 5 GHz, preventing simultaneous suppression of both ports at 6.5 GHz. The difference between measured and simulated isolation levels mainly reflects limitations in the material model used to reproduce the prototype. Although the fabricated 3 × 3 sample shows periodic fluctuations caused by finite-array effects and edge interactions; the dominant behavior remains accurately captured by the periodic unit-cell model. In our previous passive ferrite–patch study [8], infinite-periodic simulations and finite-array experiments showed close qualitative agreement with only minor edge-related deviations. Since the same electromagnetic mechanism governs the present design, unit-cell simulation provides a sufficient basis for interpreting the measured trends, even without a full-array model that includes all active components. For clarity, the design evolution is summarized here. The passive ferrite–patch structure inherently provides nonreciprocity around 6.5 GHz, achieving approximately −20 dB of isolation. Building on this baseline, two active schemes

https://doi.org/10.1017/S1759078726102888 Published online by Cambridge University Press

Table 1. Comparison of active nonreciprocal metasurfaces

	This work	[6]	[7]	[18]
Structure	Ferrite, metal patch array	Planar antenna, metasurface	Magnetic metasurface	Plasmonic, nonlinear layer
Activation Method	PIN diode	Amplifier	Self-biased ferrite	Gain + nonlinearity
Frequency band	6 GHz band	∼5.9GHz	∼15GHz	Near-IR
Nonreciprocity level	○ (11–24 dB)	◎ (12–21 dB)	○ (77% trans.)	◎ (unity contrast)
Control type	◎ (2-mode)	○ (ON–OFF)	△ (passive)	× (intensity dep.)
Simplicity	◎	×	△	×

were developed. (i) In the phase-control mode, the PIN diode adjusts the effective series impedance while preserving the forward path, yielding about 30° of transmission-phase tuning with isolation above −10 dB. (ii) In the ON–OFF mode, widening the patch forms a bidirectional stopband when the diode is ON, while the OFF state retains nonreciprocity. Although FR4 permittivity variations shift the stopband in practice, both states display clear nonreciprocal behavior with isolation around −10 dB. These step-by-step modifications show how the design progresses from passive operation to two distinct active nonreciprocal mechanisms.

Comparison with previous nonreciprocal metasurfaces

Table 1 summarizes recent representative studies on active nonreciprocal metasurfaces. Compared to prior works using transistors or nonlinear materials [18], the proposed structure offers a simple and compact design by integrating ferrite and PIN diodes into a conventional patch array. It achieves dual-mode controllability with practical performance in the microwave band.

Conclusion

In this study, we evaluated the feasibility of active phase control in a nonreciprocal metasurface previously reported by our group. Using PIN diode-based current control, we successfully achieved a transmission phase difference while maintaining nonreciprocal behavior at the same operating frequency. In addition, for ON–OFF control of nonreciprocity, the differences observed between the design and experimental results allowed us to identify key considerations for future design improvements. These findings have provided an important design direction toward the realization of phase-controllable nonreciprocal metasurfaces. Future challenges include improving the magnitude of phase shift and maintaining high transmission levels in the phase-control approach. For the ON–OFF control approach, it will be necessary to eliminate the effects of substrate manufacturing variability and to optimize the structure to be less sensitive to such variations. In addition to these device-level challenges, future work includes extending the dual-control concept to larger arrays and higher-frequency bands, reducing insertion loss through material and matching optimization, and exploring integration with practical wireless platforms such as adaptive isolation or reconfigurable shielding systems. Based on the insights gained from this study, we aim to further optimize the metasurface design in our future work.

Competing interests. The authors declare none.

References

1. **Arnmanee P** (2018) Gain improvement of microstrip patch antenna using octagonal-loop metasurface superstrate and octagonal-shaped EBG structure. In *2018 15th International Conference on Electrical Engineering/Electronics, Computer, Telecommunications and Information Technology (ECTI-CON)*, Jul. 2018, pp. 21–24. https://doi.org/10.1109/ECTICon.2018.8619919.
2. **Mishra G, Nazeer ST, Baghel S, Joy V and Singh H** (2022) Metasurface-based thin radar absorbing structure for RCS reduction in X-band. In *2022 IEEE 19th India Council International Conference (INDICON)* Jan. 2022, pp. 1–4. https://doi.org/10.1109/INDICON56171.2022.10040128.
3. **Sibille A** (2021) MIMO links mediated by reconfigurable intelligent surfaces. In *2021 15th European Conference on Antennas and Propagation (EuCAP)*. Mar. 2021, pp. 1–5. https://doi.org/10.23919/EuCAP51087.2021.9411034.
4. **Kumar S, Mishra R and Harish AR** (2023) Null steering using reconfigurable intelligent surfaces. In *2023 IEEE Microwaves, Antennas, and Propagation Conference (MAPCON)*, Feb. 2023, pp. 1–4. https://doi.org/10.1109/MAPCON58678.2023.10464045.
5. **Omar AA, Shen Z and Huang H** (2017) Absorptive frequency-selective reflection and transmission structures. *IEEE Transactions on Antennas and Propagation* **65**(11), 6173–6178. https://doi.org/10.1109/TAP.2017.2754463
6. **Taravati S, Khan BA, Gupta S, Achouri K and Caloz C** (2017) Nonreciprocal nongyrotropic magnetless metasurface. *IEEE Transactions on Antennas and Propagation* **65**(7), 3589–3597. https://doi.org/10.1109/TAP.2017.2702712
7. **Yang W, Qin J, Long J, Yan W, Yang Y, Li C, Li E, Hu J, Deng L, Du Q and Bi L** (2023) A self-biased non-reciprocal magnetic metasurface for bidirectional phase modulation. *Nat Electron* **6**(3), 225–234. https://doi.org/10.1038/s41928-023-00936-w
8. **Takahagi K and Tennant A** (2024) Experimental verification of nonreciprocal electromagnetic metasurface in a finite-size array. *Electronics Letters* **60**(12), e13240. https://doi.org/10.1049/ell2.13240
9. **Takahagi K and Tennant A** (2024) Nonreciprocal metasurfaces analyzing temperature characteristics. In *2024 18th European Conference on Antennas and Propagation (EuCAP)*, Mar. 2024, pp. 1–4. https://doi.org/10.23919/EuCAP60739.2024.10501100.
10. **Takahagi K and Tennant A** (2025) Investigation toward activating nonreciprocal metasurfaces. In *2025 19th European Conference on Antennas and Propagation (EuCAP)*, Mar. 2025, pp. 1–4. https://doi.org/10.23919/EuCAP63536.2025.10999468.
11. **Pozar DM** (2011) *Microwave Engineering*, *Fourth Edition*. Hoboken, NJ: John Wiley & Sons.
12. **Linkhart DK** (2014) *Microwave Circulator Design, Second Edition*. London: Artech House.
13. **Cerveny M, Ford KL and Tennant A** (2021) Reflective switchable polarization rotator based on metasurface with PIN diodes. *IEEE Transactions on Antennas and Propagation* **69**(3), 1483–1492. https://doi.org/10.1109/TAP.2020.3026883

https://doi.org/10.1017/S1759078726102888 Published online by Cambridge University Press

14. **Leingthone MM and Hakem N** (2018) Reconfigurable switched-beam antenna using cylindrical bow tie FSS window. In *2018 IEEE International Symposium on Antennas and Propagation & USNC/URSI National Radio Science Meeting*, Jul. 2018, pp. 1851–1852. https://doi.org/10.1109/APUSNCURSINRSM.2018.8609231.
15. **Marcuvitz N** (1951) *Waveguide Handbook*. the MIT Radiation Laboratory: IET.
16. **SureshKumar TR, Venkatesh C, Salil P and Subbarao B** (2015) Transmission line approach to calculate the shielding effectiveness of an enclosure with double-layer frequency selective surface. *IEEE Transactions on Electromagnetic Compatibility* **57**6, 1736–1739. https://doi.org/10.1109/TEMC.2015.2453333
17. **Mumby SJ and Yuan J** (1989) Dielectric properties of FR-4 laminates as a function of thickness and the electrical frequency of the measurement. *Journal of Electronic Materials* **18**(2), 287–292. https://doi.org/10.1007/BF02657420
18. **Guo T and Argyropoulos C** (2022) Nonreciprocal transmission of electromagnetic waves with nonlinear active plasmonic metasurfaces. *Physical Review B* **106**(23), 235418. https://doi.org/10.1103/PhysRevB.106.235418

https://doi.org/10.1017/S1759078726102888 Published online by Cambridge University Press